Lithospheric mantle evolution monitored by overlapping large igneous provinces: case study in southern Africa.

F. Jourdan[a*], H. Bertrand[b], G. Féraud[c], B. Le Gall[d], M.K. Watkeys[e]

[a]*Western Australian Argon Isotope Facility, Department of Applied Geology & JdL-CMS, Curtin university of Technology, GPO Box U1987, Perth, WA 6845; Australia.*

[b]*UMR-CNRS 5570, Ecole Normale Supérieure de Lyon et Université Lyon 1, 69364 Lyon, France*

[c]*UMR-CNRS 6526 Géosciences Azur, Université de Nice-Sophia Antipolis, O6108 Nice, France*

[d]*UMR-CNRS 6538, Institut Universitaire Européen de la Mer, 29280, Plouzané, France,*

[e]*School of Geological and Computer sciences, University of Natal. Republic of South Africa*

* f.jourdan@curtin.edu.au

Keywords : Large igneous province ; lithospheric mantle, mantle sources, Umkondo, Karoo, mantle plume.

Abstract

Most of the studies on the large igneous provinces (LIPs) focus on Phanerozoic times and in particular those related to the disruption of Pangea (e.g. CAMP, Karoo, Parana-Etendeka,) while Precambrian LIPs (e.g. Ventersdorpf, Fortescue) remain less studied. Although the investigation of Precambrian CFBs is difficult because of their poorly preserved character, assessing their chemical composition in parallel with younger overlapping LIP is fundamental for monitoring the evolution of the mantle composition through time.

Recent $^{40}Ar/^{39}Ar$ dating of the Okavango giant dyke swarm (and related sills) showed that ~ 90% of the dykes were emplaced at 179 ± 1 Ma and belong to the Karoo large igneous

province whereas ~10% of dykes yielded Proterozoic ages (~1-1.1 Ga). Here, we provide new major, trace and Rare Earth element analyses of the low-Ti Proterozoic Okavango dyke swarm (PODS) that suggest, combined with age data, a cognate origin with the 1.1 Ga Umkondo large igneous province (UIP).

The geochemical characteristics of the PODS and UIP basalts are comparable to those of overlapping low-Ti Karoo basalts and suggest that both LIPs were derived from similar enriched mantle sources. A mantle plume origin for these LIPs is not easily reconciled with the chemical dataset and the coincidence of two compositionally similar mantle plume acting 900 Myr apart is unlikely. Rather, we propose that the Umkondo and Karoo large igneous provinces monitored the slight evolution of a shallow enriched lithospheric mantle from Proterozoic to Jurassic.

Keywords: Large igneous provinces, Continental flood basalts, Lithospheric mantle, Umkondo, Karoo, Geochemistry.

1. Introduction

The Continental Flood Basalts (CFB) consist of large volume of magma (on the order of several million km^3) emplaced over a relatively brief time span. Whereas most of the studies focus on the Phanerozoic CFBs and particularly those related to the Pangea disruption (e.g. CAMP, Karoo-Ferrar, Parana-Etendeka, Deccan; see for instance Hawkesworth et al., 1999 and, Courtillot and Renne, 2003), Precambrian CFBs such as Ventersdorpf, Fortescue, Umkondo (Eriksson, 2002; Ernst and Buchan, 2003) remain less studied. Precambrian CFBs are frequently highly deformed and eroded and are mostly represented by dykes, sills, layered intrusions and more rarely minor remnants of flood basalts (Ernst and Buchan, 2003). Although the investigation of Precambrian CFBs is hindered by their poorly preserved character, their study is fundamental for monitoring the evolution of the mantle composition through time. This is particularly relevant when old CFB are spatially overlapped by younger ones (Iacumin et al., 2003).

Recent geochronological studies of the Okavango giant dyke swarm (Le Gall et al., 2005) (and related sill satellites) showed that ~ 88% of the dykes were emplaced at 179 ± 1 Ma (n= 14; Le Gall et al., 2002, Jourdan et al., 2004, Jourdan et al., 2005) and belong to the Karoo large igneous province. However, it has also been demonstrated that the swarm includes ~

10% of Proterozoic dykes (Jourdan et al., 2004). The latter yielded a wide range of imprecise $^{40}Ar/^{39}Ar$ "speedy step-heating" (2-3 heating steps on few plagioclase minerals used only to discriminate Jurassic and Precambrian dykes; Jourdan et al., 2004) ages ranging from 850 to 1700 Ma. One plateau age (959 ± 5 Ma) and one weighted-mean age (983 ± 4 Ma), both possibly suffering of some Ar perturbation, approximate the emplacement age of the swarm. In addition, geochemistry was used as a discriminant tool between Jurassic and Proterozoic populations. Whereas Karoo dykes were shown to be exclusively high-Ti tholeiites (TiO_2 > 2 wt.%, the Proterozoic Okavango dyke swarm and related sills (PODS hereafter) consist only of low TiO_2 (< 2 wt.%) tholeiites. The latter are compositionally similar to the Karoo low-Ti basaltic sub-province that represents the prevailing volume of the Karoo LIP (Jourdan et al., 2007). The purpose of the initial study was to demonstrate that the Jurassic dyke swarm was emplaced following a reactivated direction, and does not represent a Jurassic pristine structure (Jourdan et al., 2004). However, poor consideration was addressed to the Proterozoic dykes and their geodynamic significance. Here, we provide new major, trace and rare earth elements analyses of the Precambrian dykes. We will discuss two hypotheses for the PODS origin: (1) it is part of the recently discovered 1.1 Ga Umkondo igneous province (UIP, Hanson et al., 1998) or (2) it belongs to a Kibaran post-orogenic rifting. In a second part, we compare the composition of the PODS and the low-Ti Karoo Jurassic magmatism in order to monitor the evolution of the underlying mantle through time.

2. Geological setting and samples descriptions

The N110°-trending giant Okavango dyke swarm and related sills intrude mainly Archaean (Zimbabwe craton) and Proterozoic (e.g. the Magondi belt) rocks and the metamorphic Limpopo-Shashe belt (Le Gall et al., 2002). The swarm is crosscut at high angle by the ~100 km long dry Shashe River, allowing efficient sampling. From the 77 rocks sampled along the Shashe River and surroundings, 11 were assigned to the Proterozoic, based on their speedy step-heating ages and major element composition (Jourdan et al., 2004). Eight dykes and 2 sills were sampled along the Shashe River and 1 sill (Bot0003) comes from further south of the swarm (Fig. 1).

Whereas the dimension of the Jurassic dyke swarm is relatively well constrained by aeromagnetic survey (~1500 x 100 km; Reeves et al., 2000; Chavez Gomez, 2001), the extension of the Proterozoic swarm remains unknown, because it is virtually impossible to

differentiate between the two swarms by aero-magnetic measurements (Tshoso et al., 2002; Aubourg et al., 2008). Along the Shashe river (the only section allowing a systematic sampling across the dyke swarm), $^{40}Ar/^{39}Ar$ dating coupled with geochemistry (Jourdan et al., 2004) show that Proterozoic dykes represent ~10 % of the ODS and are mostly restricted within a 20 km-wide corridor located in the center of the ODS (Fig. 1b-c). The Proterozoic dykes inside the Shashe River vary in thickness from 4 to 20 m. The three sills investigated consist of small elongated and rounded sheets of dolerites located in the Shashe River (Bot11 and Bot01) and in eastern Botswana (Bot0003; Fig. 1b,c).

The Proterozoic dykes and sills consist of fine to medium grained olivine-free dolerites with an ophitic to sub-ophitic texture. They contain mostly plagioclase and pyroxene (augite and pigeonite) with minor Ti-magnetite and pyrite. Amphibole occurs in almost all samples (except the two sills Bot11 and Bot0003) as replacement of the pyroxene, suggesting the occurrence of a weak low-grade greenshist metamorphism. Amphibole is sometimes accompanied by minor biotite. The alteration phases are mostly chlorite and sericite. The modal composition of the Proterozoic dykes is not easily distinguishable from that of the Jurassic dykes of the Okavango swarm. The most reliable discriminant seems to be amphibole which is not observed in Karoo dolerites except in rare more differentiated samples (Jourdan et al., 2004). However, the existence of Proterozoic amphibole-free rocks makes this criteria somewhat misleading.

3. Geochemistry

The eleven Proterozoic samples were analyzed for major, trace and rare earth (REE) elements (Table 1). They were crushed and powdered in an agate miller. Major and trace elements were determined on fused disc and pressed powder pellets, respectively and were analyzed by XRF (Philips PW 1404 spectrometer) at University of Lyon. REE, U and Th were measured at the Chemex University (Canada). Analytical uncertainties vary from 1% to 2% and from 10% to 20% for major and trace elements respectively, depending on the concentration of the element.

The eight dykes and three Proterozoic sills have low TiO_2 (0.5-2.1 wt.%) and low P_2O_5 (0.03-0.23 wt.%) contents (Fig. 2). They are quartz- or olivine-normative tholeiites. SiO_2 and alkali contents range from 48.9 to 54.3 wt.% and from 2.3 to 4 wt.%, respectively. They are classified as basalts and basaltic-andesites in the TAS diagram (Le Bas et al., 1986; not

shown). MgO and Mg# [100 x Mg/(Mg+Fe^{2+}), considering Fe_2O_3/FeO =0.15] vary from 3.9 to 8.2 wt.% and from 34 to 63, respectively, indicating the moderately evolved character of the rocks (Fig. 2). Mg# exhibits a negative co-variation with SiO_2, Na_2O and TiO_2, and a positive co-variation with CaO and Al_2O_3 (Fig. 2). These trends suggest that dolerites have been affected by differentiation processes involving fractional crystallization. The Proterozoic rocks can be subdivided into two sub-groups: (i) a group including 3 samples with relatively moderate TiO_2 and SiO_2 contents (≥ 1.7 wt.% TiO_2 and ≤ 52.1 wt.% SiO_2) and with a low Mg# (≤ 47), and (ii) a group of 8 samples with lower TiO_2 and higher SiO_2 contents (≤ 1wt.% TiO_2 and ≥ 52.5wt.% SiO_2; Fig. 2) and with a Mg# > 47. Hereafter these two groups are referred to as the high- and low-Mg# groups, respectively. The low-Mg# sub-group includes two sills (Bot01 and Bot11) and one dyke (Bot15) from the Shashe River and thus the difference between the two groups cannot be related to the nature of the intrusion (i.e. sill or dyke). Moreover, it is unlikely that the chemical difference between the groups was produced by different degrees of alteration as the discriminant elements do not co-vary with LOI contents which are relatively low in the two groups (0.5 to 1.4 wt.%).

The two sub-groups mentioned above display distinct trends on most trace elements plots (Fig.3). The amount of incompatible (e.g. Rb, Y) and compatible (e.g. Cr) trace elements increases and decreases, respectively, as Mg# decreases, in accordance with fractional crystallization within each sub-group. The PODS have low Ce/Pb values (from 0.5 to 5.8), largely lower than the accepted values for OIB and MORB (~25; Chauvel et al., 1995) and plots in the field of subduction-related rocks.

On the multi-elements normalized diagrams, the Proterozoic dolerites show a moderate enrichment in the most incompatible trace elements (ITE; Rb/Y_n = 6-34 Fig. 4). The patterns are characterized by negative anomalies for Nb (Nb/Nb* = 0.18-0.43), Sr (Sr/Sr* = 0.28-0.71), P (P/P* = 0.53 to 0.79) and Ti (Ti/Ti* = 0.54 to 0.90) which are more pronounced for the high-Mg# sub-group. The REE patterns (Fig.5) show a relatively slight Light REE (LREE) enrichment compared to Heavy REE (HREE; La/Yb_n = 3.3-4.4) and a poor HREE fractionation (Sm/Yb_n = 1.5-1.7). A slight negative anomaly in Eu (Eu/Eu* = 0.70-0.92) concurs with the Sr anomaly as an indication of plagioclase fractionation.

The dyke compositions display no chemical variation across the width of the swarm. The sills have indistinguishable composition compared to the dykes.

4. Discussion

4.1. Petrogenesis of the PODS

4.1.1. Partial melting

Equilibrium non-modal melting has been modeled by using the standard equation of Shaw (1967). In order to explain the poor fractionation of the Middle REE (MREE) and HREE, we used a garnet-free, spinel bearing lherzolite (< 80 km depth) with the same modal composition as used by Jourdan et al. (2007) for the Karoo low-Ti basalts (55% olivine, 15% orthopyroxene, 28% clinopyroxene and 2% spinel). A slightly more enriched source composition has been chosen to account for the small difference between PODS and Karoo rocks (La/Yb_{source}=3.27 and 2, respectively). Partition coefficients are from McKenzie and O'Nions (1991). We reported the melting curves in the $(La/Yb)_n$ vs. $(Eu/Yb)_n$ and $(Sm/Yb)_n$ vs. $(La/Sm)_n$ plots (Fig. 6). The calculated melts, produced in the range of 5-10% melting, adequately match the observed REE variations. The low-Mg# group requires a higher melting rate (9-10 %) compared to the high-Mg# group (5-8%), in order to fit the lower $(La/Sm)_n$ values of the former group.

4.1.2. Fractional crystallization

Petrographic observations and major and REE element behavior show that the PODS rocks cannot be considered as primary mantle melts and that they underwent fractional crystallization of gabbroic assemblages. MELTS algorithm (Ghiorso and Sack, 1995; Smith and Asimow, 2005) calculates the liquid lines of descent of magmas and provides the composition of both residual liquids and cumulate minerals. We carried out isobaric runs using various pressures (P=0.5-5 Kbars) and H_2O contents (H_2O=0-2 wt. %) conditions (e.g. Fig. 7) and fO_2=QFM (quartz-fayalite-magnetite). We used one of the less differentiated sample as starting composition (Bot0003; Mg# = 66). The homogeneous composition of the PODS hinders the best estimate of the run conditions, yet the fractional crystallization at low pressure (1-2 Kbars) under anhydrous conditions satisfactorily fits the high-Mg# group. The amount of fractionation (up to ~80 %) of a gabbroic assemblage (clinopyroxene + plagioclase) seems however too high to be realistic, ruling out that the data spread can be

explained by fractional crystallization alone. The low-Mg# group shows much more dispersion of the sample compositions but does not include enough samples (n=3) to allow fractional crystallization modeling. In any case, this group requires different source starting conditions (higher degree of partial melting (Fig. 6) or different source composition?) to be accounted for.

Minor variations within the data set not accounted for by differentiation processes could be best explained by the contribution of (1) small crustal contamination, but this is hard to verify in absence of isotope data and/or (2) weak hydrothermal alteration (if present) that may have happened during the low grade metamorphism phase. In addition, the starting composition assumed in this model is not a primary magma and does not take into account earlier fractionating assemblages which can explain substantial differences among the samples if several magma chambers are involved.

In summary, a combination of partial melting of a common mantle source and subsequent fractionation processes may account for most of the variations of the PODS samples. However, minor alteration, crustal contamination or mantle source heterogeneity (or any combination of the three) seems also to be required to account for some of the observed discrepancies.

4.2. Mantle source of the PODS

The geochemical characteristics of the low-Ti PODS are similar to those reported for low-Ti Phanerozoic CFB (e.g. Karoo-Ferrar, CAMP, Parana-Etendeka). For instance, the rocks are enriched in ITE and in LREE relatively to HREE and display a strong Nb anomaly. The mantle sources at the origin of CFBs are yet not well resolved with models ranging from mantle plume head (Morgan, 1981; White and McKenzie, 1989; Campbell and Griffiths, 1990; Hill, 1991; Wilson, 1997, Courtillot et al., 1999) to the sub-continental lithospheric mantle (SCLM; Hawkesworth et al., 1984, 1999; Bertrand, 1991; Molzahn and Reisberg 1996; Jourdan et al., 2003, 2007) or perispheric mantle (Anderson et al., 1992, 1994). Some authors have suggested that each CFB is more or less distinctive and that the origin of these provinces cannot be explained by a unique "dogmatic" model (e.g. Hawkesworth et al., 1999; Jourdan et al., 2007). For instance, the Deccan (Peng et Mahoney, 1995) or Ethiopia-Yemen (Pick et al., 1999) traps fit particularly well the deep mantle plume model as suggested by their OIB-like elemental and isotopic geochemistry, whereas the Karoo mantle sources are

more likely located either partially or totally in the SCLM (e.g. Sweeney et al., 1994; Molzahn and Reisberg., 1996; Jourdan et al., 2007).

The La/Nb-La/Ba plot is commonly used to investigate the origin of CFB rocks (Fig. 8, Saunders et al., 1992; Hawkesworth et al., 1999, Nomade et al., 2002, Jourdan et al., 2007) and is particularly relevant when isotopic analyses are not available. Positive correlations between La/Nb and La/Ba reflect OIB and/or asthenospheric mantle source(s) whereas negative correlations are diagnostic of a strong lithospheric contribution. These ratios are almost not modified by petrogenetic processes (Hawkesworth et al., 1999) and thus, likely represent mantle source signature(s). The PODS rocks display a similar mantle trend as the Karoo magmas (Jourdan et al., 2007), though with a shallower slope. Both groups point toward relatively low La/Ba and high La/Nb values. Following Saunders et al. (1992), we interpret these values as indicating a strong contribution from the SCLM. Similarly, the Zr/Y-Ti/Y plot (Fig. 9) shows that the PODS rocks are clustered between the bulk earth composition and a "post-Archaean shale" component. This pole has been commonly interpreted as representing a subducted sediment signature (Brewer et al., 1992 and references inside) possibly located in the SCLM. Two samples align themselves on the primitive mantle/MORB – OIB array, in direction of the OIB field. This might be interpreted as a potential evidence of a small contribution of a lamproitic or a mantle plume component in the genesis of these two rocks, but the evidences are tenuous.

As mentioned above, the Ce/Pb (0.5-5.8; Fig. 3) is by far too low to reflect OIB or MORB mantle (Ce/Pb>20; e.g. Chauvel et al., 1995) and is closer in composition to subduction-related magmas (Ce/Pb<10). Although the PODS do not display calc-alkaline characteristics, fluids released from a previous subduction may have "polluted" the SCLM (Hawkesworth et al., 1999). Concerning the two PODS sub-groups (i.e. low- and high-Mg#), their similarities in ITE and REE patterns and concentrations, and their behavior in discriminant diagrams strongly suggest that they are issued from a similar mantle source. The difference between the two groups is mostly expressed by P, Ti and Nb anomaly. However, these anomalies are neither correlated with the Mg# nor with the LREE/HREE variations (not shown), suggesting that these differences are not due to fractionation or melting processes. Therefore, we suggest that these differences might be induced by small scale heterogeneities of a common mantle source.

In summary, the PODS rocks are hardly assigned to an OIB-like asthenospheric or mesospheric mantle source model (i.e. mantle plume; Campbell and Griffiths, 1990) neither to a calk-alkaline subduction-related magmatism (despite common features as low Ce/Pb and

Nb anomaly). The best source candidate suggested by our data is therefore likely to be located in the lithospheric mantle (La/Nb>2) metasomatically enriched by a previous subduction event (Zr/Y~6-7, Ce/Pb<10). A 1.4-1.3 Ga subduction event (Kibaran subduction) has been reported in the Namaqua orogenic belt (Kampunzu et al., 2000 and references therein) and was suspected to have been responsible for the enriched signature of the 1.1 Ga Kwebe within plate volcanism (Fig. 10; Kampunzu et al., 2000). We speculate that the Kibaran subduction may have been also responsible for the PODS and related sills mantle source enrichment. Crucial isotopic analyses would be required for assessing this hypothesis.

4.3. Geodynamic setting of the PODS?

4.3.1. Age of the PODS

The PODS samples yielded "speedy step-heating" ages ranging from 850 to 1700 Ma (Jourdan et al., 2004). This age range does not reflect an extremely long-lasting geological process but is induced by the poor constraints inherent to the speedy step-heating method which cannot resolve the complex interaction between alteration and excess of Ar (Jourdan et al., 2004). A plateau and a weighted-mean ages of 983 ± 4 (sample Bot0083) and 959 ± 5 Ma (sample Bot0003) were obtained on plagioclase-separates using standard step-heating method (Jourdan et al., 2004).

The younger sample has a flat $^{37}Ar_{ca}/^{39}Ar_K$ spectrum, apparently indicative of a negligible alteration. On the other hand, the older sample shows a strongly tilde-shaped $^{37}Ar_{Ca}/^{39}Ar_K$ that can be attributed either to important alteration (Verati and Féraud, 2003) or to strong mineral zoning. When plagioclase has been altered into a significant amount of sericite (i.e. > 20 %), this can produce statistically valid but spuriously young "alteration" plateau ages due to the large K content of sericite (K_2O ~10 wt.%) compared to plagioclase (~0.05 wt.%). In any case, it is not clear whether these ages represent crystallization ages or a partial/total reset of the isotopic system by a subsequent low-degree metamorphism (as evidenced by amphibolitisation of the pyroxene phenocrysts).

For comparison, $^{40}Ar/^{39}Ar$, K/Ar and Rb/Sr ages obtained so far on the basic Mesoproterozoic CFB-related rocks from southern-Africa/Antarctica (Umkondo large igneous province (UIP); Fig. 10) appear to be strongly perturbed with ages ranging from 600 ± 24 to 1802 ± 100 Ma (Kruger et al., 2000; Key and Ayers, 2000; Reimold et al., 2000; Burger and Valreven, 1979 and 1980). In contrast, robust zircon and baddeleyite U/Pb TIMS ages obtained on the same

298 formations (plus additional rocks from different localities) are restricted between 1106.1 ± 2.0
299 and 1112.0 ± 0.5 Ma (Shwartz et al., 1996; Hanson et al, 1998, 2004, 2006; Singletary et al.,
300 2003). This suggests that rocks emplaced during the Mesoproterozoic period suffered strong
301 perturbations that so far preclude the use of the K/Ar, Rb/Sr and even $^{40}Ar/^{39}Ar$
302 geochronometers for investigating their crystallization ages.
303 In absence of further evidence on the meaning of the $^{40}Ar/^{39}Ar$ ages obtained in Jourdan et al.
304 (2004), we could propose two different hypotheses; (1) these ages reflect
305 alteration/metamorphism processes with strong perturbation of the $^{40}Ar/^{39}Ar$ chronometer and
306 thus the magmatism is likely to be substantially older (possibly as old as and belonging to the
307 1.1 Ga Umkondo magmatism; Hanson et al., 1998 and 2004), or (2) these dates are true
308 crystallization ages and are possibly representative of a distention process associated to the
309 late-Kibaran orogeny (1.0 Ga), In the following parts, we test these two hypotheses.
310
311 *4.3.2. Post-Kibaran failed rift dykes hypothesis*
312
313 The "Kibaran" Mesoproterozoic belt stretches over 3000 km long through central and
314 southern Africa. The Kibaran belt is a broad patchwork of smaller similarly aged belts. It is
315 located along the eastern and southern part of the Congo craton (Fig. 10; Kampunzu et al.,
316 1998; Kokonyangi et al., 2004). Between 1.4 and 1.0 Ga, Kibaran metasedimentary and
317 igneous rocks were involved in two compression events (Johnson and Oliver, 2000) that
318 cannot be truly dissociated into 2 distinct orogens (Kampunzu et al., 1998). The Kibaran
319 orogeny includes an active continental margin (Kibaran orogeny sensu stricto, 1.4-1.2 Ga)
320 followed by a continental collision (Namaquan orogeny; 1.1-1.0 Ga). The late stage of the
321 Namaquan orogeny was marked by numerous granitic intrusions, which yielded Rb-Sr
322 isochron ages ranging from 966 ± 21 to 1006 ± 44 Ma (Cahen and Ledant, 1979; Cahen et al,
323 1984; Ikingura et al. ,1990) and U/Pb ages on zircon separate at 1.02-1.0 Ga (Singletary et al.,
324 2003). Very few examples of major dyke swarm emplaced in compressive environments
325 exist. Féraud et al. (1987) identified alkaline dykes linked with the Indo-European, African
326 and Arabian plate collision. These dykes are narrow (0.5 to few meters wide) and follow the
327 direction of the maximum horizontal compressive stress. Another example is given by the
328 ~700 km- long Independence dyke swarm, occurring throughout southeastern California in
329 relation to the subduction of the Farallon plate beneath the North American plate (Chen and
330 Moore, 1979; Coleman et al., 2000). The Independence swarm shows a typical bimodal arc-
331 magmatism-type composition (e.g. Coleman et al., 2000; Jourdan et al., 2005) and is

emplaced perpendicular to the direction of the subducting plate and to the main compressive stress vector.

The PODS is roughly located at high-angle to the Kibaran belt, following its maximum compressive vector, and could therefore represent a direct expression of the Kibaran orogeny. However, two points argue against this hypothesis: (1) the PODS dykes are substantially thicker than those mentioned in pure collisional settings (Féraud et al., 1987), (2) they do not exhibit an alkaline or a calc-alcaline composition as expected in a compressive system, but a typical CFB composition not commonly reported in an orogenic context.

4.3.3. Comparison between PODS and the Umkondo igneous province

Recent paleomagnetic and geochronological (mainly zircon U/Pb analyses) investigations suggest a common origin to Proterozoic tholeiites occurring throughout the southern Africa and possibly Antarctica (Fig. 10; Hanson et al., 2004). These terms are regrouped as the Umkondo igneous province (UIP), given from the name of Umkondo Zimbabwe dolerite formation of the same age. The UIP is now defined as a widespread Mesoproterozoic continental flood basalt emplaced in southern Africa and Antarctica (Hanson et al., 1998 and 2004). It consists of tholeiitic mafic intrusions (sills and dyke swarms) and scarce remnants of eroded basaltic lava-flows emplaced over an estimated paleo-surface of ~$2.5 \cdot 10^6$ km² (Fig. 10). This igneous event is contemporaneous but not directly related to the collision of the Laurentia and Kalahari cratons (Grenville-Llano and Namaqua-Natal Orogeny) which contributed to the formation of the Rodinia mega-continent (Hanson et al., 1998; Dalziel et al., 2000).

Robust ages clustered around 1.1 Ga have been obtained using zircon and baddeleyite U/Pb TIMS technique (Hanson et al., 1998 and 2004). Unfortunately, contrary to geochronological data, complete sets of major, trace and rare earth elements are still scarce and restricted to few outcrops. We therefore compare the PODS only to the 1105 ± 2 Ma Zimbabwe Umkondo dolerites (eastern Zimbabwe; Munyaniwa, 1999), the geochemically-related Guruve and Mutare dykes (Northern Zimbabwe; Ward et al., 2000), although several generations of dykes might be involved in this swarm (Hanson et al., 2006) and the 1108.6 ± 1.2 Ma Anna rust's sheet (South Africa; Reimold et al., 2000 and references herein) (Fig. 10). The bimodal (acidic and basic) sequence from Kwebe (western Botswana) yielded U-Pb zircon ages of 1106 ± 2 Ma and 1104 ± 16 Ma (Schwartz et al., 1996) but these rocks are not considered

here because their chemical composition present a large scatter due to alteration and greenschist metamorphism (Kampunzu et al., 1998) .

The UIP dolerites are mostly low-Ti basaltic rocks (TiO_2 = 0.4-1.9 wt.%; except two high-Ti samples) and are moderately evolved rocks with SiO_2 and Mg# mainly ranging from 48.8 to 57.0 wt.% and from 45 to 63, respectively. They show a moderate ITE enrichement (Rb/Y_n = 3.0-33.1) and a variable negative Nb anomaly (33 samples range from 0.12 to 0.95). Five rocks from Kwebe (Kampunzu et al., 1998), 1 dyke from Mutare (Ward et al., 2000) and 1 dolerite from Zimbabwe (Munyaniwa, 1999) exhibit a positive Nb anomaly ranging from 1.14 to 2.28. However, it is not clear if the positive Nb anomaly feature is pristine or if it is due to secondary K loss (K is used to in this study to calculate the Nb anomaly) during the slight greenshist metamorphism. UIP dolerites display moderate REE fractionation mainly concerning light REE (La/Ybn = 1.7-7.7; La/Sm_n = 1.3 to 4.3). Ce/Pb is low and varies from 1.6 to 7.3 for all the rocks. Compared to the PODS, the Umkondo dolerites share striking similar characteristics. They display important overlap in major (Fig. 2) and trace (Fig. 3) elements with for instance similar correlations between Mg# and TiO_2, SiO_2, Al_2O_3 and CaO and between Zr and Y (not shown). Both groups show noticeable dominant Nb and Sr anomaly and a low Ce/Pb ratio (<8). PODS and UIP are also characterized by a moderately enriched ITE patterns (Fig. 4a, 4b) and REE (Fig. 5a, 5b) with unfractionated HREE. In the Zr/Y-Ti/Y diagram (Fig. 9), most of the UIP and PODS rocks overlap pointing mainly toward post Archaean shale component (except three outlier samples trending toward a high Ti/Y component).

In order to compare the genesis of UIP and PODS rocks, the former were reported on the melting modeling diagram (Fig.6). They strikingly plot on the same modeled curves as the PODS and can be reproduced by a wider range (1.5 to 15 %) of melting of the same spinel lherzolite source (Fig. 6). The only two high-Ti UIP dolerites identified so far, also match the (2wt. %) garnet-bearing curve calculated by Jourdan et al. (2007) for the Karoo high-Ti basalts.

The only significant difference between UIP and POD samples is shown by the Ba/Nb vs. La/Nb plot (Fig. 8). The UIP rocks are subdivided into two groups showing different trends. The Umkondo dolerites from Zimbabwe display the same negative trend as the PODS rocks, pointing toward a lithospheric component whereas the Anna rust's sheet apparently follows a positive (asthenospheric-like) correlation trend.

In summary, although the PODS might have been triggered by the intrusion of magma in relation to the Kibaran compressional orogeny, it is more likely to be related to a CFB event

399 as monitored by its geochemical data. The only known CFB occurring at the end of the
400 Mesoproterozoic is the Umkondo magmatism. The Umkondo rocks share strikingly similar
401 composition with the PODS samples, thus arguing for the same mantle source. However, it is
402 still not clear if this mantle source has been tapped at two different periods or in a few Myr
403 time span. As the apparent ages obtained on PODS are possibly perturbed, the simplest
404 explanation would be that the PODS was emplaced contemporaneously to the UIP (1.1 Ga)
405 and may have a cognate magmatic origin. However, further dating based on robust zircon
406 and/or baddeleyite U/Pb analyses are required to test this hypothesis.
407
408 *4.4. Overlapping Umkondo and Karoo CFBs: a witness of SCLM evolution through time?*
409
410 The partial geographical overlap of Umkondo and Karoo CFBs (Fig. 1 and 10) provides a
411 good opportunity to test whether these two provinces share a similar mantle source or not. In
412 addition, the former case would allow to assess to what extent this common mantle source
413 may have evolved ~900 Myr apart, from 1.1 Ga to 180 Ma.
414 Since four decades, the Karoo magmatism was chemically investigated by various authors
415 (e.g. Cox, 1967; Hawkesworth et al., 1984; Sweeney et al., 1994; Jourdan et al., 2007). Data
416 gleaned through these studies show that the Karoo magmatism, as most of the CFBs, consists
417 of low- and high-Ti basalts (Cox, 1988). Although some authors have proposed a OIB-like
418 mantle plume origin for the Karoo magmatism (Ellam et al., 1992), a vast majority of workers
419 argue for a dominant contribution of a subduction-modified SCLM (e.g. Duncan et al., 1984;
420 Cox, 1988, Sweeney and Watkeys, 1990; Sweeney et al., 1994; Hawkesworth et al., 1999;
421 Elburg and Goldberg, 2000 Jourdan et al., 2007) with heat source provided by mechanisms
422 such as supercontinent shield effect (Coltice et al., 2007 and submitted)
423 Here, we compare the geochemistry of the Proterozoic UIP, exemplified by the low-Ti
424 PODS, to Jurassic low-Ti Karoo basalts from Botswana and Zimbabwe (Jourdan et al., 2007
425 and references insides). High-Ti rocks will not be considered here, as they are unknown in the
426 PODS, so far and are represented by only two samples in the UIP. These two CFB provinces
427 share many similar features. Both groups show a significant overlap concerning most of the
428 major (Fig. 2) and trace (Fig. 3) elements. They display similar enriched ITE patterns (Fig. 4).
429 All but seven (see discussion above) UIP samples bear a negative Nb anomaly ranging from
430 0.12 to 0.95 that compares to 0.22 to 0.81 for the low-Ti Karoo basalts. Both provinces have
431 REE patterns that show moderately fractionated LREE (La/Yb_n = 2.0 to 3.4 for Karoo low-Ti

basalts vs. 1.7-7.7 for UIP low-Ti basalts) but unfractionated mid-REE vs. HREE (Sm/Yb_n from 1.2 to 1.6 for Karoo vs. 1.3-1.9 for UIP; Fig. 5).

However, significant differences distinguish the Proterozoic from the Jurassic basalts. In general, PODS rocks have higher SiO_2 and ITE (e.g. Rb) contents and slightly lower contents for other major and compatible elements (e.g. TiO_2 and Cr; Fig. 2, 3), for a given Mg#. The most striking differences concern the ITE patterns, which display pronounced negative Sr, P and Ti anomalies for the PODS basalts but not for the Karoo low-Ti basalts (Fig. 4). The UIP also display more pronounced negative Nb anomalies as well as slightly lower Ce/Pb ratios in average (Fig. 3). On the Zr/Y vs. Ti/Y diagram (Fig. 9) the trend toward the shale component is more pronounced for the PODS than for Karoo low-Ti basalts. Globally, the PODS shows stronger subduction characteristics than the Karoo basaltic rocks (e.g. Nb anomaly, Ce/Pb, low Ti/Y and high La/Nb).

We further test if the Karoo and PODS low-Ti rocks have a similar mantle source by comparing their batch melting model curves (Fig. 6). The Karoo trend is reproduced by 3 to 20 % melting of a slightly more depleted mantle source (La/Yb = 2 against 3.27 for UIP) and using the same modal composition compared to the PODS (Jourdan et al., 2007). The two curves are almost overlapping, strongly attesting for a similar, although not identical mantle source for the two CFBs.

Therefore, the data suggest that the PODS and the Karoo low-Ti basaltic rocks originate from enriched mantle sources that bear very close characteristics. These two magma suites show strong and dominant SCLM mantle signatures (e.g. low Ce/Pb and important Nb negative anomalies). Considering the 900 Myr interval between the two CFB events, the differences observed between the Proterozoic and Jurassic rocks are tenuous. They can be interpreted in term of (1) lateral and vertical heterogeneities in the SCLM, (2) evolution of the SCLM from 1.1 Ga to 180 Ma or a combination of both. Consequently, hypothesis (2) would imply that the (subduction-enriched?) SCLM underwent only a slight depletion since Proterozoic times. Such depletion might be due to extraction of the widespread Umkondo CFB. In that case, the enriched composition of the SCLM would be already established before the 1.1 Ga Umkondo event. This proposition is strengthened as the Karoo rocks show a noticeable decoupling between $^{206}Pb/^{204}Pb$ and $^{207}Pb/^{204}Pb$ which was interpreted by Jourdan et al. (2007) as reflecting the contribution of a stable and old-enriched mantle source. As mentioned above, and also proposed for Ferrar rocks from Droning Maud Land (Lutinen and Furnes, 2000), the chemical enrichment of the source was suggested to represent a feature inherited from a Proterozoic orogeny, possibly the 1.4-1.3 Ga Kibaran subduction (Kampunzu

et al., 1998). A similar approach has been conducted for the Late Archaean-Proterozoic (2.7 and 1.0 Ga) and Mesozoic (200 and 130 Ma) CFB magmatism in South America and concluded also for only a slight evolution of the composition of the SCLM through time (Iacumin et al., 2003).

These results have important bearing on the mantle plume issue at the origin of Umkondo and Karro CFBs. As discussed above, no mantle plume signature is recognized in the PODS and UIP dataset. Moreover the mantle plume hypothesis for both UIP and Karoo would assume that two distinct plume heads sharing similar compositions would have been emplaced 900 Myr apart, coming from laterally distinct source regions (considering the drift of the African plate from 1.1Ma to 180Ma). It is unlikely that these requirements were fulfilled, and we favor the persistence of a SCLM source slightly evolving through time.

Further work is required to monitor the evolution of the LIP mantle source through time in southern Africa. This includes isotopic analysis on the PODS to highlight the similarities and differences with the Karoo province, and investigation of Proterozoic and Archaean dykes of other dykes swarms (e.g. Save-Limpopo, Olifant River and Palabora dyke swarms; Jourdan et al., 2006).

5. Conclusions

The geochemical investigations on the mafic Proterozoic Okavango dyke swarm and related sills (PODS) lead us to draw several conclusions:

(1) Geochemical characteristics (e.g. Nb anomaly, Ce/Pb ratio, ITE and REE pattern) suggest that the PODS was derived from the melting of a shallow mantle source. This source is different from the OIB or MORB mantle and is thought to represent sub-continental lithospheric mantle (SCLM) enriched by fluids released during the 1.4-1.3 Ga Kibaran subduction.

(2) The PODS shares similar geochemical characteristics with basaltic remnants scattered in Botswana, Zimbabwe and South Africa and attributed to the 1.1 Ga Umkondo large igneous province (UIP). Considering younger ~1 Ga disturbed Ar/Ar ages previously obtained, the PODS is considered as either part of the UIP or issued from a UIP-like source reactivated ~100 Myr later.

(3) The PODS and UIP CFB overlap and share similar characteristics with the 180 Ma low-Ti Karoo CFB. Modeling suggests that both were derived from melting of a similar but not

identical enriched spinel-bearing mantle source. The resemblance between these Proterozoic and Jurassic CFBs supports the tapping, 900 Ma apart, of a common enriched stabilized SCLM attached to the African plate and is hard to reconcile with the melting of two distinct mantle plumes. The slight depletion of the Karoo basalts relatively to the PODS suggests that the extraction of the Umkondo magmas from the SCLM may have contributed to its relative depletion. The southern African SCLM therefore inherited its characteristics since the Mesoproterozoic and has probably undergone no major enrichment since this period.

Acknowledgments

This work is part of a partnership between the University of Botswana and the French Universities of Nice, Lyon and Brest. We acknowledge the financial support of the CNRS (grant INSU Intérieur de la Terre), the French Ministry of Foreign Affairs, the University of Botswana (Grant RPC Kaapvaal Craton Project R#442), the SU-CRI 2E of the University of Western Brittany and the Universities of Nice and Lyon. We are grateful to C. Tonani, Head of the Cultural and Scientific Service of the French Embassy in Botswana for his support in developing this program. M. Manetti and P. Capiez are thanked for analytical assistance. FJ thanks E. Eroglu for discussion. Géosciences Azur contribution No. 433.

References

Anderson, D.L., Zhang, Y. S., Tanimoto, T., 1992. Plume heads, continental lithosphere, flood basalts and tomography. In: B.C. Storey, Alabaster, T., Pankhurst, R.J. (Eds), Magmatism and the Causes of Continental Break-up. Special Publication of the Geological Society of London, pp. 99-124.

Anderson, D.L., 1994. The sublithospheric mantle as the source of continental flood basalts; the case against the continental lithosphere and plume head reservoirs. Earth and Planetary Science Letters 123, 269-280.

Aubourg, C., Tshoso, G., Le Gall, B., Bertrand, H., Tiercelin, J.-J., Kampunzu, A.B., Dyment, J., Modisi M., 2008. Magma flow revealed by magnetic fabric in the Okavango giant dyke swarm, Karoo igneous province, northern Botswana. Journal of Volcanology and Geothermal Research 170, 247–261.

Bertrand, H., 1991. The Mesozoic tholeiitic provinces of northwest Africa: a volcano-tectonic record of the early opening of Central Atlantic. In: A.B. Kampunzu, Lubala, R.T. (Eds), Magmatism in extensional structural settings. The Phanerozoic African plate. Springer-Verlag, Berlin Heigelbert, New York, pp. 147-188.

Boynton, W.V., 1984. Geochemistry of the rare earth elements: meteorite studies. In: Henderson P. (Ed), Rare earth element geochemistry. Elsevier, pp. 63-114.

Brewer, T.S., Hergt, J.M., Hawkesworth, C.J., Rex, D and Storey, B.C., 1992. Coats Land dolerites and the generation of Antarctic continental flood basalts. In: B.C. Storey, Alabaster, T., Pankhurst R.J. (Editor), Magmatism and the causes of continental break up. Geological Society Special Publication, pp. 185-208.

Burger, A.J., Walraven, F., 1979. Summary of age determinations carried out during the period April 1977 to March 1978. South Africa Geological Survey Annals, 12: 209-218.

Burger, A.J., Walraven, F., 1980. Summary of age determinations carried out during the period April 1978 to March 1979. South Africa Geological Survey Annals, 14: 109-118.

Cahen, L., Ledent, D., 1979. Précision sur l'age, la pétrogenèse et la position stratigraphique des "granites à étain" de l'est de l'Afrique Centrale. Bulletin Société Belge Géologiques, 88: 33-49.

Cahen, L., Delhal, J., Vail, J.R., Bonhomme, M., Ledent, D., 1984. The geochronology and evolution of equatorial Africa. Clarendon Press, Oxford, 496pp.

Campbell, I.H., Griffiths, R.W., 1990. Implications of mantle plume structure for the evolution of flood basalts. Earth and Planetary Science Letters 99, 79-73.

Chauvel, C., Goldstein, S.L., Hofmann, A.W., 1995. Hydration and dehydration of oceanic crust controls Pb evolution in the mantle. Chemical Geology 126, 65-75.

Chavez Gomez, S., 2001. A catalogue of dykes from aeromagnetic surveys in eastern and southern Africa. ITC publication number 80.

Coltice, N., Phillips, B.R., Bertrand, H., Ricard, Y., Rey, P., 2007. Global warming of the mantle at the origin of flood basalts over supercontinents. Geology 35, 391-394.

Coltice, N., Bertrand, H., Rey, P., Jourdan, F., Philipps, B.R., Ricard Y., Global warming of the mantle beneath continents back to the Archean; submitted to Gondwana Research.

Courtillot, V., Jaupart, C., Manighetti, I. Tapponnier, P., Besse, J., 1999. On causal links between flood basalts and continental breakup. Earth and Planetary Science Letters 166, 177-195.

Courtillot, V.E., Renne, P. R., 2003. On the ages of flood basalt events. Comptes Rendus Geosciences 335, 113-140.

565 Cox, K.G., MacDonald, R., Hornung, G., 1967. Geochemical and petrogenetic provinces in
566 the Karroo basalts of southern Africa. American Mineralogist 52, 1451-1474.
567 Cox, K.G., 1988. The Karoo Province. In: J.D. MacDougall (Ed), Continental Flood Basalts.
568 Kluwer, Boston, pp. 239-271.
569 Dalziel, I.W.D., Mosher, S., Gahagan, L.M., 2000. Laurentia-Kalahari collision and the
570 assembly of Rodinia. The Journal of Geology 108, 499-513.
571 Duncan, A.R., Erlank, A.J., Marsh, J.S., 1984. Regional geochemistry of the Karoo ingeous
572 province. In: A.J. Erlank (Editor), Petrogenesis of the volcanic rocks of the Karoo
573 province. Geological Society Special Publication of South Africa., pp. 355-388.
574 Elburg, M., Goldberg, A., 2000. Age and geochemistry of Karoo dolerite dykes from
575 northeast Botswana. Journal of African Earth Sciences 31, 539-554.
576 Ellam, R.M., Carlson, R.W., Shirley, S.B., 1992. Evidence from R-Os isotopes for plume-
577 lithosphere mixing in Karoo flood basalt genesis. Nature 359, 718-721.
578 Eriksson, P.G., Condie, K.C., Van der Westhuizen, W., Van der Merwe, R., De Bruiyn, H,
579 Nelsond, D.R., Altermanna, W., Catuneanue, O., Bumbya, A.J., Lindsayf, J.,
580 Cunninghama, M.J., 2002. Late Archaean superplume events: a Kaapvaal-Pilbara
581 perspective. Journal of Geodynamics 34, 207-247.
582 Ernst, R.E., Buchan, K.L., 2003. Recognizing mantle plumes in the geological record. Annual
583 Review of Earth and Planetary Sciences 31, 469-523.
584 Féraud, G., Giannérini, G., Campredon, R., 1987. Dyke swarms as paleostress indicators in
585 areas adjacent to continental collision zones: examples from the European and northwest
586 Arabian plates. In: H.C. Halls, Fahrig, W.F. (Eds), Mafic dyke swarms. Geological
587 Association of Canada Special Paper, pp. 273-278.
588 Hanson, R.E., Martin, M.W., Bowring, S.A., Munyanyiwa, H., 1998. U-Pb zircon age for the
589 Umkondo dolerites, eastern Zimbabwe: 1.1 Ga large igneous province in southern Africa-
590 East Antarctica and possible Rodinia correlations. Geology 26, 1143-1146.
591 Hanson, R.E., Crowley, J.L., Bowring, S. A., Ramezani, J., Gose, W.A., Dalziel, I.W. D.,
592 Pancake, J. A., Seidel, E. K., Blenkinsop, T. G., Mukwakwami, J., 2004. Coeval large-
593 scale magmatism in the Kalahari and Laurentian cratons during Rodinia assembly.
594 Science 304, 1126-1129.
595 Hanson, R.E., Harmer, R.E., Blenkinsop, T.G., Buller, D.S., Dalziel, I.W.D., Gose, W.A.,
596 Hall, R.P., Kampunzu, A.B., Key, R.M., Mukwakwami, J., Munyanyiwa, H., Pancake,
597 J.A., Seidel, E..K., Ward, E.K., 2006. Mesoproterozoic intraplate magmatism in the
598 Kalahari Craton: A review. Journal of African Earth Sciences 46, 141-167.

599 Hawkesworth, C., Kelley, S., Turner, S., Le Roex, A., Storey, B., 1999. Mantle processes
600 during Gondwana break-up and dispersal. Journal of African Earth Sciences 28, 239-261.
601 Hawkesworth, C.J., Marsh, J.S., Duncan, A.R., Erlank, A.J., Norry, M.J., 1984. The role of
602 continental lithosphere in the generation of the Karoo volcanic rocks: evidence from
603 combined Nd- and Sr-isotope studies. In: A.J. Erlank (Ed), Petrogenesis of the volcanic
604 rocks of the Karoo province. Geological Society Special Publication of South Africa., pp.
605 341-354.
606 Hill, R.I., 1991. Starting plume and continental break-up. Earth and Planetary Science Letters
607 104, 398-416.
608 Iacumin, M., De Min, A., Piccirillo, E. M., Bellieni, G., 2003. Source mantle heterogeneity
609 and its role in the genesis of Late Archaean-Proterozoic (2.7-1.0 Ga) and Mesozoic (200
610 and 130 Ma) tholeiitic magmatism in the South American Platform. Earth-Science
611 Reviews 62, 365-397.
612 Ikingura, J.R., Bell, K., Watkinson, D.H., Van Straaten, P., 1990. Geochronology and
613 chemical evolution of granitic rocks, NE Kibaran (Karagwe-Ankolean) belt, NW
614 Tanzania. In: G. Rocci, Deschamps, M. (Ed), Recent Data in African Earth Sciences.
615 International Center for Training and Exchanges in the Geosciences Occasional
616 Publication, pp. 97-99.
617 Jonhson, S.P., Oliver, G.J.H., 2000. Mesoproterozoic oceanic subduction, island arc
618 formation and the initiation of back-arc spreading in the Kibaran Belt of central, southern
619 Africa: evidence from the Ophiolite Terrane, Chewore Inliers, northern Zimbabwe.
620 Precambrian Research 103, 2000.
621 Jourdan, F., Marzoli, A., Bertrand, H., Cosca, M., Fontignie., D., 2003. The northernmost
622 CAMP: Ar/Ar age, petrology and Sr-Nd-Pb isotope geochemistry of the Kerforne dyke,
623 Brittany, France. In: W. Hames, J.G. McHone, C. Rupel, P.R. Renne (Ed), The Central
624 Atlantic Magmatic Province. A.G.U. Monograph, pp. 209-226.
625 Jourdan, F., Féraud, G., Bertrand, H., Kampunzu, A.B., Tshoso, G., Le Gall, B., Tiercelin,
626 J.J., Capiez P., 2004. The Karoo triple junction questioned: evidence from $^{40}Ar/^{39}Ar$
627 Jurassic and Proterozoic ages and geochemistry of the Okavango dyke swarm (Botswana).
628 Earth and Planetary Sciences Letters 222, 989-1006.
629 Jourdan, F., Renne, P.R., Mundil, R., 2005. $^{40}Ar/^{39}Ar$ and U/Pb Ages and geochemistry of the
630 Benton Range Dike Swarm, SE California: New Evidence for an “Independence” Poly-
631 phased Dike Swarm, in: Geophysical research abstract, AGU fall meeting

632 Jourdan, F., Féraud, G., Bertrand, H., Watkeys, M.K., Kampunzu, A.B., Le Gall B., 2006.
633 Basement control on dyke distribution in Large Igneous Provinces: case study of the
634 Karoo triple junction, Earth and Planetary Science Letters 241, 307-322.
635 Jourdan F., Bertrand, H., Sharer, U., Blichert-Toft, J., Féraud, G., Kampunzu, A.B., Le Gall,
636 B., Watkeys, M.K., 2007. Major and Trace Element and Sr, Nd, Hf, and Pb Isotope
637 Compositions of the Karoo Large Igneous Province, Botswana-Zimbabwe: Lithosphere vs
638 Mantle Plume Contribution. Journal of Petrology 48, 1043-1077
639 Kampunzu, A.B., Akanyang, P., Mapeo, R.B.M., Modie, B.N., Wendorff, M., 1998.
640 Geochemistry and tectonic significance of the Mesoproterozoic Kgwebe metavolcanic
641 rocks in northwest Botswana: implications for the evolution of the Kibaran Namaqua-
642 Natal belt. Geological Magazine 135, 669-683.
643 Kampunzu, A.B., Armstrong, R.A., Modisi, M.P., Mapeo, R.B.M., 2000. Ion microprobe U-
644 Pb ages on detrital zircon grains from the Ghanzi Group: implication for the identification
645 of Kibaran-age crust in northern Botswana. Journal of African Earth Sciences 30, 579-
646 587.
647 Key, R.M., Ayres, N., 2000. The 1998 edition of the National Geological Map of Botswana.
648 Journal of African Earth Sciences 30, 427-451.
649 Kokonyangi, J., Armstong, R., Kampunzu, A.B., Yoshida, M., Okudaira, T., 2004. U-Pb
650 zircon geochronology and petrology of granitoids from Mitwaba (Katanga, Congo):
651 implications for the evolution of the Mesoproterozoic Kibaran belt. Precambrian Research
652 132, 79-106.
653 Kruger, F.J., Geringer, G.J., Havenga, A.T., 2000. The geology, Petrology, geochronology
654 and source region character of the layered gabbronoritic Orangekom Complex in the
655 Kibaran Namaqua mobile belt, South Africa. Journal of African Earth Sciences 30, 667-
656 687.
657 Le Bas, M.J., Le Maitre, R.W., Streickeisen, A., Zanettin, B., 1986. A chemical classification
658 of volcanic rocks based on the total alkali silica diagram. Journal of Petrology 27, 745-
659 750.
660 Le Gall, B., Tshoso, G., Jourdan, F., Féraud, G., Bertrand, H., Tiercelin, J.J., Kampunzu, A.B.
661 Modisi, M.P., Dyment, M., Maia, J., 2002. $^{40}Ar/^{39}Ar$ geochronology and structural data
662 from the giant Okavango and related mafic dyke swarms, Karoo igneous province,
663 Botswana. Earth and Planetary Science Letters 202, 595-606.
664 Le Gall B., Tshoso, G., Dyment, J. Kampunzu, A. B., Jourdan, F., Féraud, G., Bertrand, H., &
665 Aubourg, C., 2005. The Okavango giant mafic dyke swarm (NE Botswana) and its

666 structural significance within the Karoo Large Igneous Province. Journal of Structural
667 Geology 27, 2234-2255.
668 Luttinen, A.V., Furnes, H., 2000. Flood basalts of Vestfjella: Jurassic magmatism across an
669 Archaean-Proterozoic Lithospheric Boundary in Droning Maud Land, Antarctica. Journal
670 of Petrology 41, 1271-1305.
671 McKenzie, D., O'Nions, R.K., 1991. Partial melt distribution from inversion of rare earth
672 element concentrations. Journal of Petrology 32, 1021-1091.
673 Molzahn, M., Reisberg, L., 1996. Os, Sr, Nd, Pb, O isotope and trace element data from the
674 Ferrar flood basalts, Antarctica: evidence for an enriched subcontinental lithospheric
675 source. Earth and Planetary Science Letters 144, 529-545.
676 Morgan, W.J., 1981. Hot spot tracks and the opening of the Atlantic an Indian Oceans. In: C.
677 Emiliani (Editor), The Sea, 7. Wiley Interscience, New York, pp. 443-487.
678 Munyanyiwa, H., 1999. Geochemical study of the Umkondo dolerites and lavas in
679 Chimanimani and Chipige Districts (eastern Zimbabwe) and their regional implications.
680 Journal of African Earth Sciences 28, 349-365.
681 Murphy, J.B., Hynes, A.J., 1986. Contrasting secondary mobility of Ti, P, Zr, Nb and Y in
682 two metabasaltic suites in the Appalachians. Canadian Journal of Earth Sciences 23, 1138-
683 1144.
684 Nomade, S., Pouclet, A., Chen, Y., 2002. The French Guyana dolerite dykes: geochemical
685 evidence of three populations and new data for the Jurassic Central Atlantic magmatic
686 province. Journal of Geodynamics 34, 595-614.
687 Peng, Z.X., Mahoney, J.J., 1995. Drillhole lavas from the northwestern Deccan Traps, and the
688 evolution of Réunion hotspot mantle. Earth and Planetary Science Letters 134, 169-185.
689 Pik, R., Deniel, C., Coulon, C., Yirgu, G., Marty, B., 1999. Isotopic and trace element
690 signatures of Ethiopian flood basalts: Evidence for plume-lithosphere. Geochimica and
691 Cosmochimica Acta 15, 2263-2279.
692 Reeves, C., 2000. The geophysical mapping of Mesozoic dyke swarms in southern Africa and
693 their origin in the disruption of Gondwana. Journal of African Earth Sciences 30, 499-513.
694 Reimold, W.U., Pybus, G.Q.J., Kruger, F.J., Layer, P.W., Koeberl, C., 2000. Anna's Rust
695 Sheet and related gabbroic intrusion in the Vredefort Dome - Kibaran magmatic event on
696 the Kaapvaal Craton and beyond? Journal of African Earth Sciences 31, 499-521.
697 Saunders, A.D., Storey, M., Kent, R.W., Norry, M.J., 1992. Consequences of plume-
698 lithosphere interactions. In: B.C. Storey, Alabaster, T., Pankhurst, R.J. (Ed), Magmatism

and the causes of continental break-up. Geological Society of London Special Publication, pp. 41-60.

Schwartz, M.O., Kwok, Y.Y., Davis, D.W., Akanyang, P., 1996. Geology, geochronology and regional correlation of the Ghanzi Ridge, Botswana. South African Journal of Geology 99, 245-250.

Shaw, D.M. (1967). Trace element fractionation during anatexis. Geochemica, Cosmochimica Acta 34, 237-234.

Singletary, S.J., Hanson, R.E., Martin, M.K., Crowley, J.L., Bowring, S.A., Key, R.M., Ramokate, L.V., Dreng, B.B., Krol, M.A., 2003. Geochronology of basement rocks in the Kalahari Desert, Botswana, and implications for regional Proterozoic tectonics. Precambrian Research 121, 47-71.

Sun, S.S., McDonough, W.F., 1989. Chemical and isotopic systematics of oceanic basalts: implication for mantle composition and processes. In: A.D. Saunders, Norry, M.J. (Editor), Magmatism in the ocean basin. Blackwell, Oxford.

Sweeney, R.J., Duncan, A.R., Erlank, A.J., 1994. Geochemistry and petrogenesis of Central Lebombo basalts from the Karoo Igneous Province. Journal of Petrology 35, 95-125.

Sweeney, R.J., Watkeys, M.K., 1990. A possible link between Mesozoic lithospheric architecture and Gondwana flood basalts. Journal of African Earth Sciences 10, 707-716.

Tshoso, G., Dyment, J., Aubourg, C., Legall, B., Tiercelin, J.J., Féraud, G., Bertrand, H., Jourdan, F., Kampunzu, A.B., 2002. Magnetic Investigations on the Okavango Giant Dyke Swarm (N Botswana). E.G.S. XXVII Geophysical Research Abstracts Nice, pp. 78.

Ward S.E., Hall, R.P., Hughes, D.J., 2000. Guruve and Mutare dykes: preliminary geochemical indication for complex Mesoproterozoic mafic magmatic systems in Zimbabwe. Journal of African Earth Sciences 30, 689-701.

White, R.S., McKenzie, D.P., 1989. Magmatism at rift zones: the generation of volcanic continental margins and flood basalts. Journal of Geophysical Research 94, 7685-7729.

Wilson, M., 1997. Thermal evolution of the Central Atlantic margins: continental break-up above a Mesozoic super-plume. Journal of Geological Society of London 154, 491-495.

Figure and table captions

Figure 1: A) Distribution of the Karoo magmatism and major related dyke swarms (modified after Jourdan et al., 2004 and references inside). ODS: Okavango dyke swarm; PODS: Proterozoic Okavango dyke swarm; ORDS: Olifants River dyke swarm; SBDS: South Botswana dyke swarm; SLDS: Sabi-Limpopo dyke swarm; SleDS: South Lesotho dyke swarm; SMDS: South Malawi dyke swarm; RRDS: Rooi Rand dyke swarm; LDS: Lebombo dyke swarm (undated, intruding Karoo lava-pile); GDS: Gap dyke swarm (undated, intruding Karoo sediments). Dotted line corresponds to Botswana border. Thick dashed line corresponds to the hypothesized limit of the Umkondo large igneous province (UIP; cf. Fig. 10). B) Sketch map of northeastern Botswana showing the N110° oriented ODS-PODS and location of Bot0003 samples. Lava flows exposures are indicated. C) 100 km-long section along the Shashe River, with the location of Proterozoic samples only (modified after Jourdan et al., 2004).

Figure 2: Selected major elements vs. Mg# [100 x atomic ratio of $Mg/(Mg+Fe^{2+})$ with Fe_2O_3/FeO normalized to 0.15]. Low-Ti Karoo basalts (Jourdan et al., 2007) and Umkondo igneous rocks (see text for references) were indicated for comparison (see discussion). The low-Mg# group is surrounded by dashed curve.

Figure 3: Selected trace elements vs. Mg#. Caption as in Figure 2.

Figure 4. Primitive mantle normalized (Sun and McDonough, 1989) incompatible trace elements patterns for (A) PODS and related sills with the low-Mg# group indicated by dashed curves (B) Umkondo igneous province (UIP; see text for references) and (3). Karoo low-Ti basalts and sills (Jourdan et al., 2007).

Figure 5. Chondrite-normalized (Boynton, 1984) REE compositions for (A) PODS and related sills with the low-Mg# group indicated by dashed curves, (B) Umkondo igneous province (UIP; see text for references) and (C) Karoo low-Ti basalts and sills (Jourdan et al., 2007).

Figure 6. $(Sm/Yb)_n$ vs. $(La/Sm)_n$ and $(La/Yb)_n$ vs. $(Eu/Yb)_n$ plots for the PODS and related sills, Karoo low- and high-Ti basalts and sills and UIP. Non-modal batch melting modeling curves of lherzolite mantle source are indicated. Partition coefficients are from McKenzie and O'Nions (1991). The ticks on the curves correspond to melting rates. Melting curve of a

766 spinel-bearing lherzolite source (modal composition 55% olivine, 15% orthopyroxene, 28%
767 clinopyroxene and 2% spinel). Melting mode: 20% olivine, 20% orthopyroxene, 55%
768 clinopyroxene, 5% spinel. PODS source preferred composition: La=1.80, Sm=0.75 Eu=0.23
769 and Yb=0.55 (black dashed curve). Karoo best-fit source composition: La=1.10, Sm=0.67
770 Eu=0.24 and Yb=0.55 (gray plain curve). The gray dashed-dotted curve represents the
771 calculated garnet-bearing mantle source as proposed in Jourdan et al. (2007), indicated for
772 comparison.
773
774 Figure 7. Al_2O_3 and CaO vs. Mg# for the basaltic samples and MELTS (Ghiorso and Sack,
775 1995) fractional crystallization modeling curves. Calculation parameters: Pressure and H_2O
776 content are varying between 0.5 Kbars and 5 Kbars and 0% and 2% respectively. fO_2=QFM
777 (quartz-fayalite-magnetite). Starting composition: rock Bot0003 (Mg# = 66); note that adding
778 H_2O in the starting rock composition shift its SiO_2 composition because the total composition
779 is normalized to 100%.
780
781 Figure 8. La/Ba vs. La/Nb plot for the PODS, UIP and Karoo low-Ti basalts and sills. Fields
782 reported as in Saunders et al. (1992).
783
784 Figure 9. Ti/Y vs. Zr/Y plot for the PODS, UIP and Karoo low-Ti basalts and sills. Fields
785 reported from Brewer et al. (1992). The low-Mg# group is indicated by a dashed curve.
786
787 Figure 10. Distribution of the 1.1 Ga Umkondo large igneous province (after Hanson et al.,
788 1988 and 2004). The locations of the samples used for geochemical comparison are quoted in
789 bold. PODS black dashed line indicates possible extension of the dyke swarm by comparison
790 with the ODS. Thin dotted line: Botswana border. Thick dashed line: schematic "Kibaran-
791 aged" belts represented with basement fabrics.
792
793 Table 1. Major (wt%) and trace and RE elements (ppm) analyses for the PODS and related
794 sills rocks. LOI: loss on ignition. Most trace elements of most samples were determined by
795 ICPMS except those quoted in italic, measured by XRF.
796

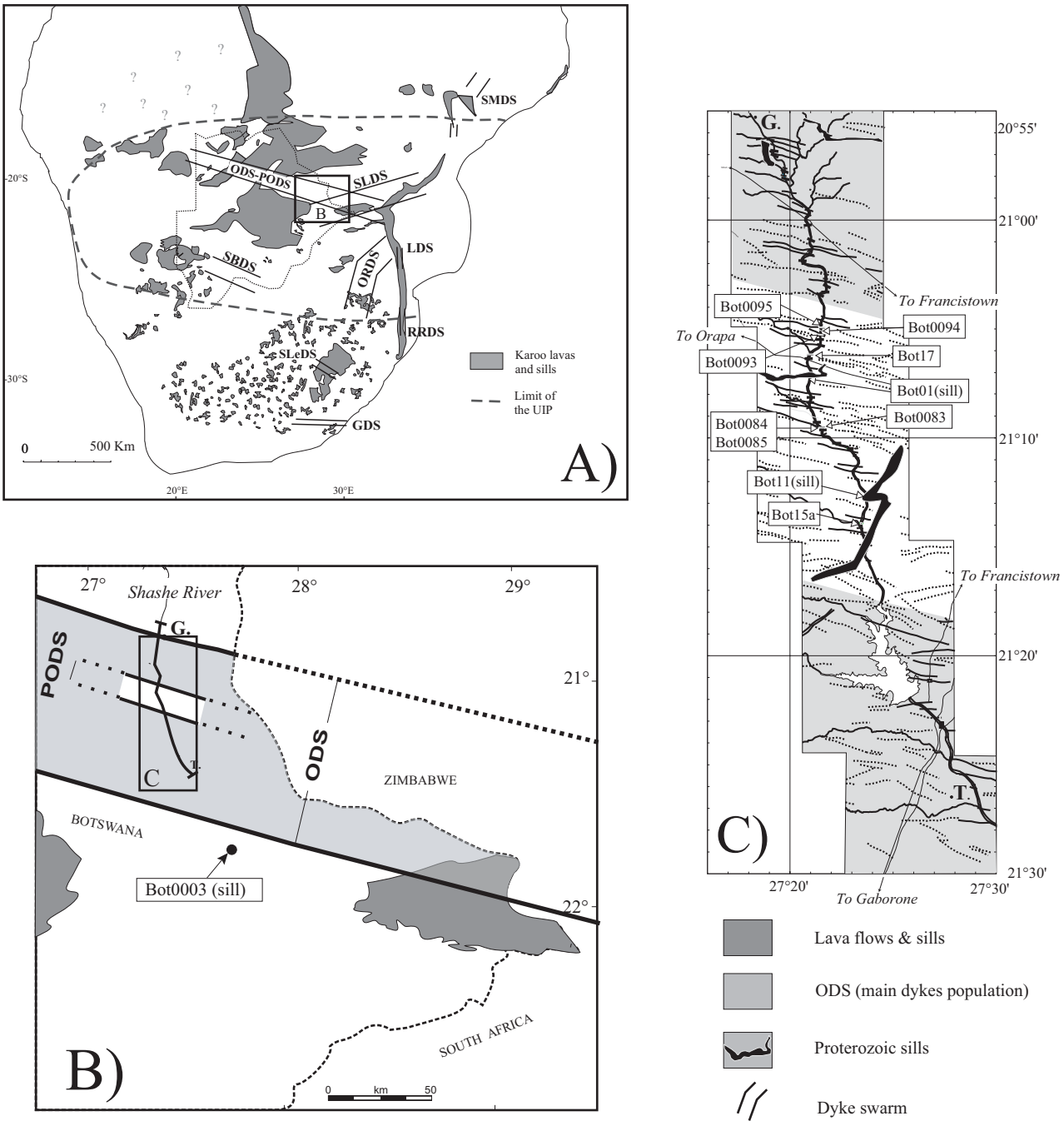
A)
SMDS
ODS-PODS
SLDS
B
LDS
SBDS
ORDS
RRDS
SLeDS
GDS
Karoo lavas and sills
Limit of the UIP
0
500 Km
20°S
30°S
20°E
30°E
B)
27°
Shashe River
28°
29°
21°
22°
PODS
ODS
G.
T.
C
ZIMBABWE
BOTSWANA
SOUTH AFRICA
Bot0003 (sill)
0
km
50
C)
20°55'
21°00'
21°10'
21°20'
21°30'
27°20'
27°30'
To Francistown
To Orapa
To Gaborone
Bot0095
Bot0094
Bot0093
Bot17
Bot01(sill)
Bot0084
Bot0085
Bot0083
Bot11(sill)
Bot15a
Lava flows & sills
ODS (main dykes population)
Proterozoic sills
Dyke swarm

Figure 1

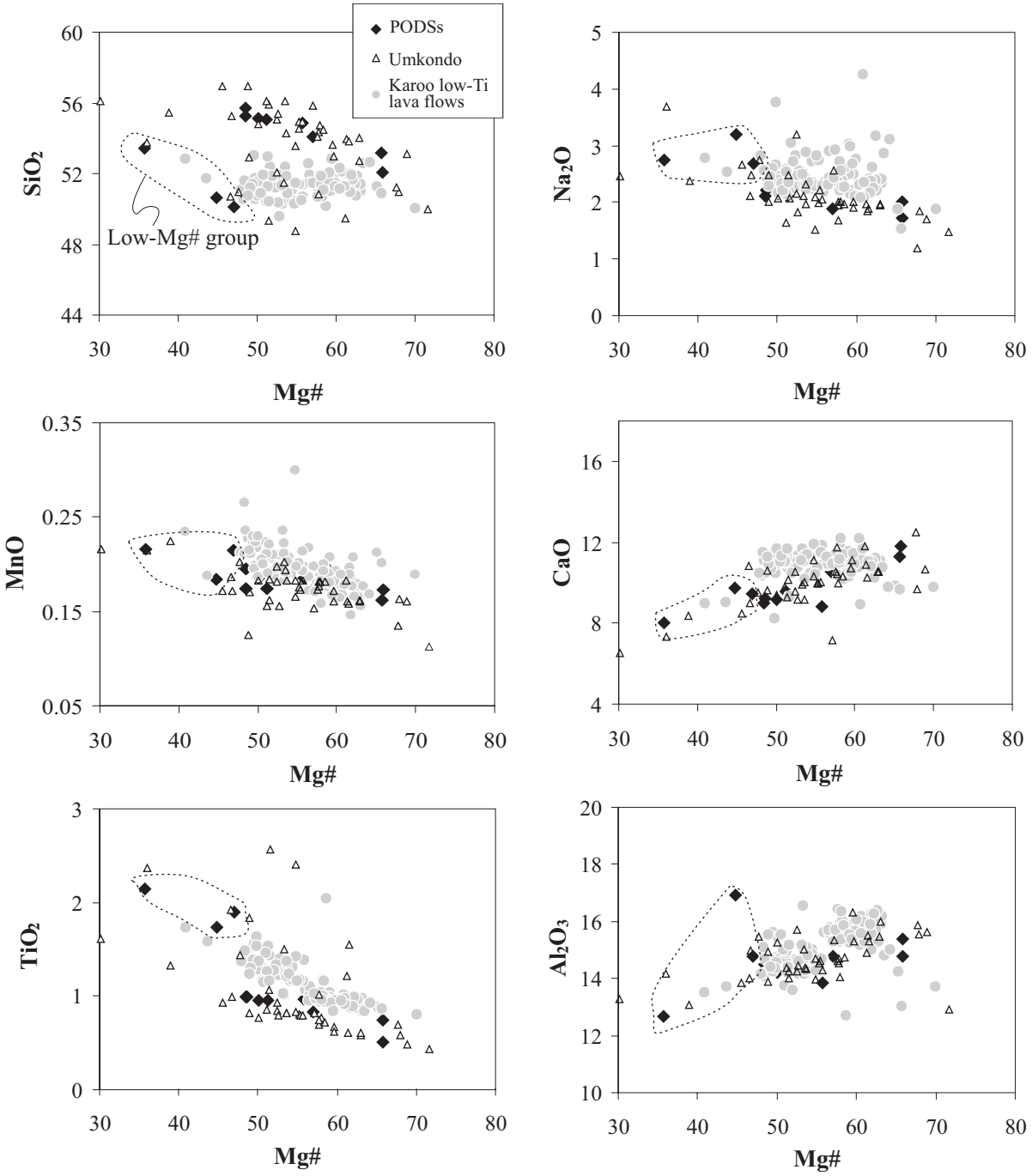
PODSs
Umkondo
Karoo low-Ti lava flows
Low-Mg# group
SiO2
Na2O
MnO
CaO
TiO2
Al2O3
Mg#

Figure 2

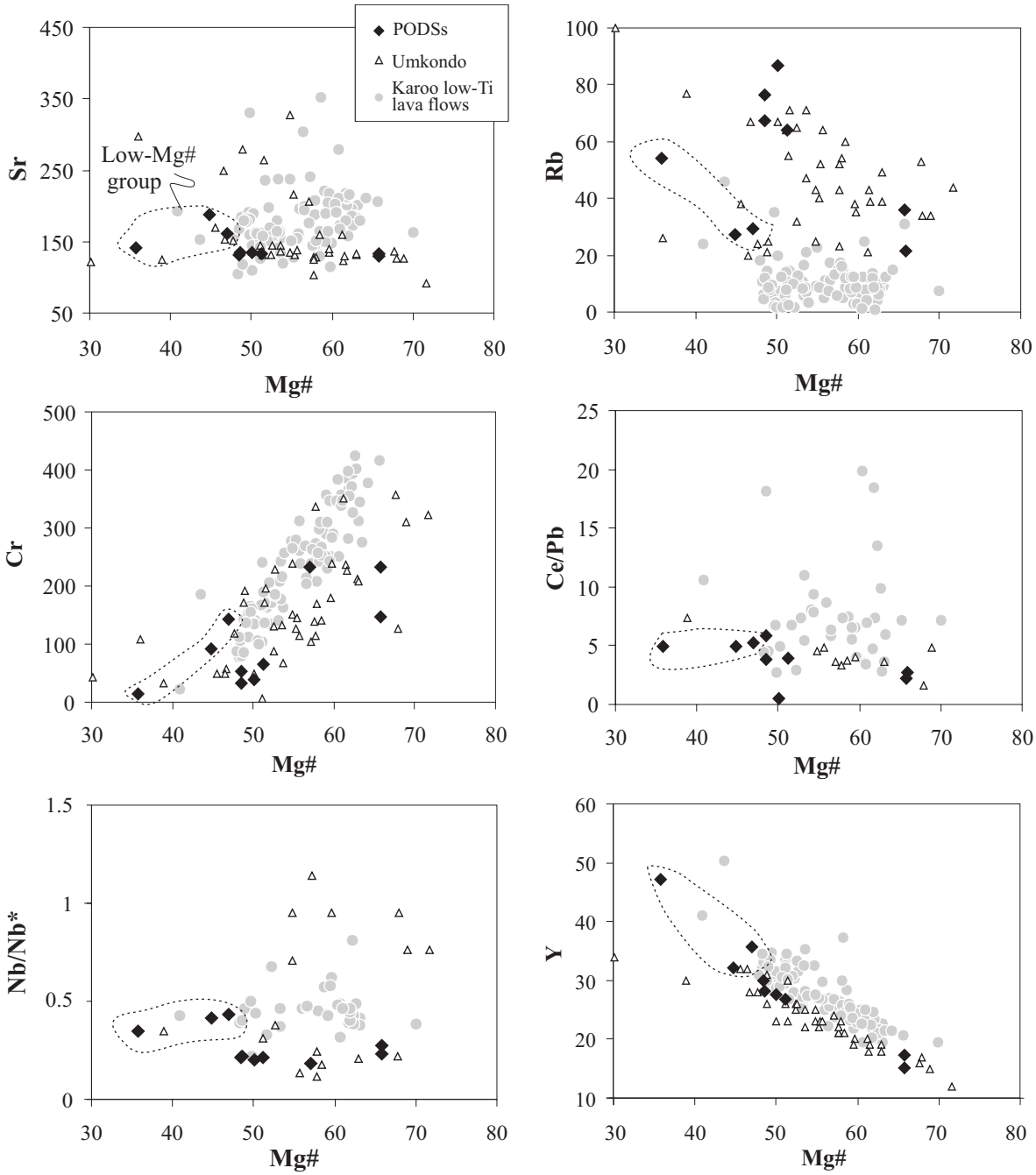
PODSs
Umkondo
Karoo low-Ti lava flows
Low-Mg# group
Sr
Rb
Cr
Ce/Pb
Nb/Nb*
Y
Mg#

Figure 3

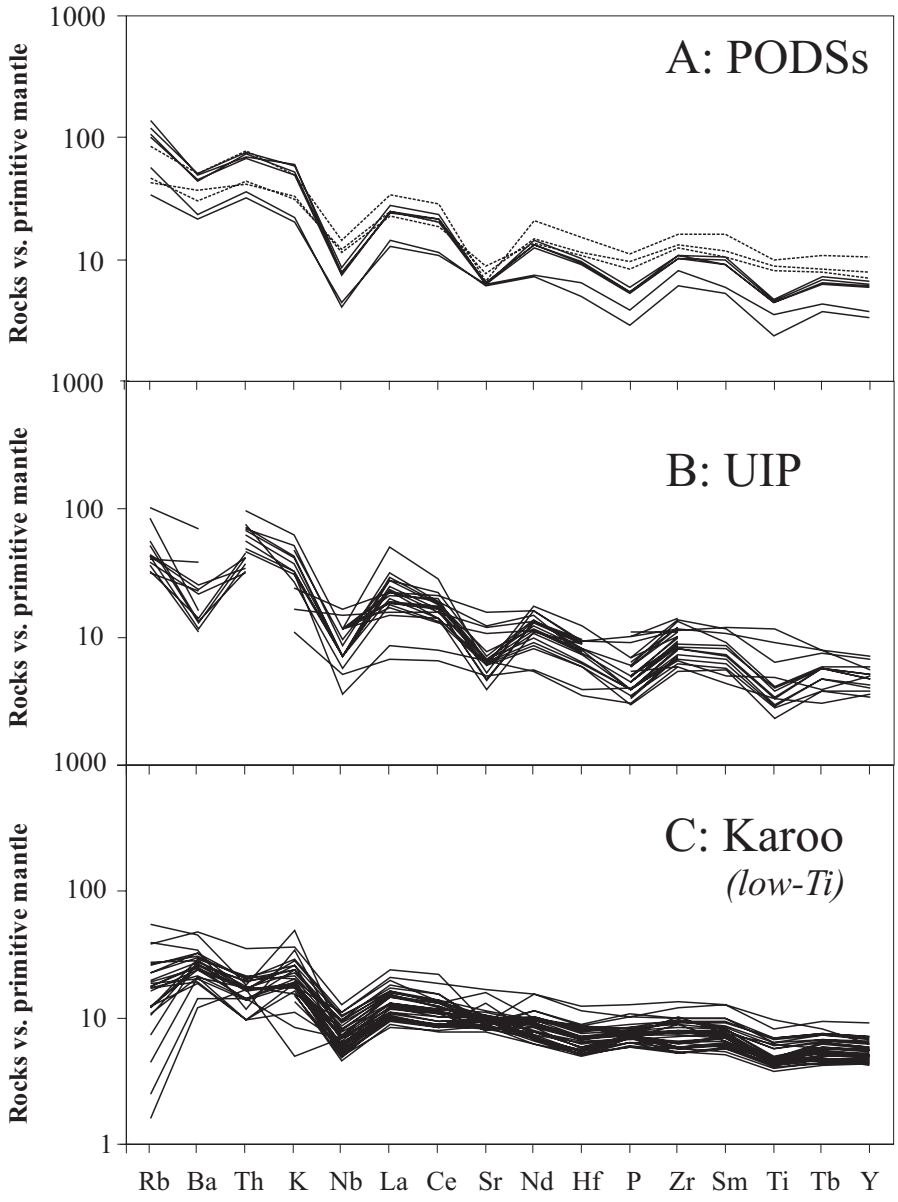
A: PODSs
B: UIP
C: Karoo
(low-Ti)
Rocks vs. primitive mantle
1000
100
10
1
Rb Ba Th K Nb La Ce Sr Nd Hf P Zr Sm Ti Tb Y

Figure 4

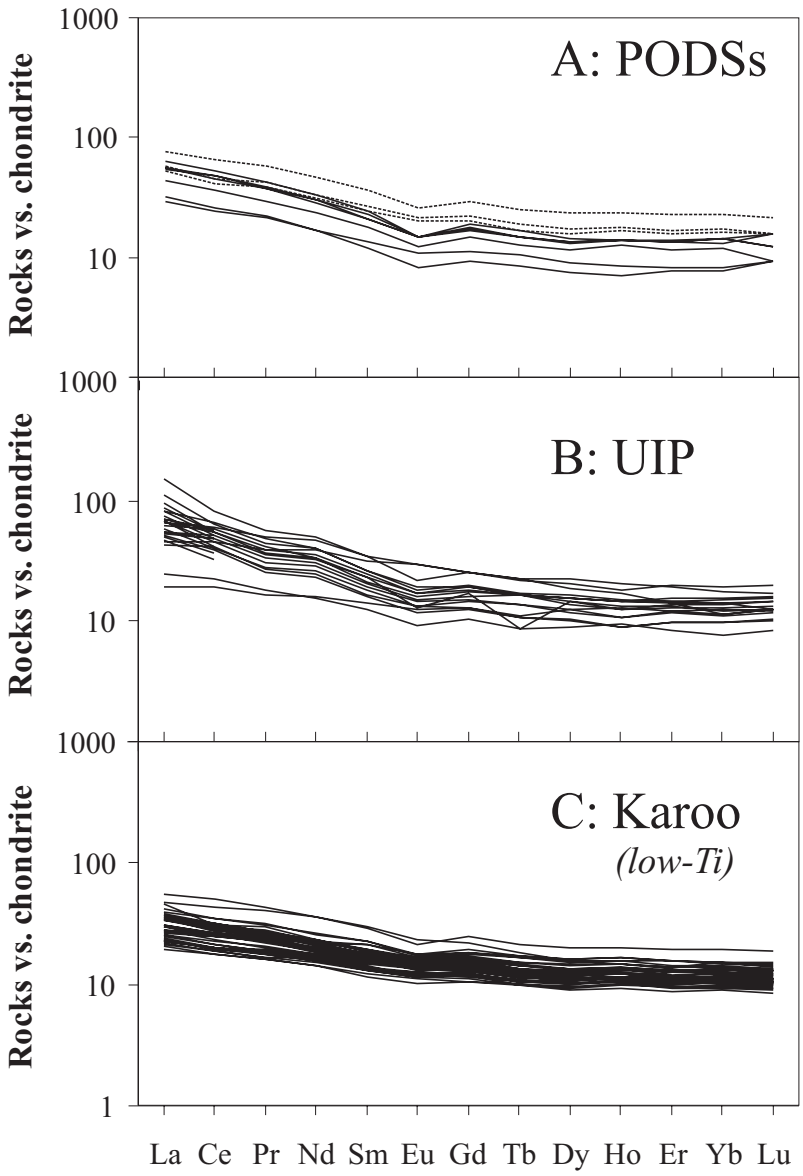
A: PODSs
B: UIP
C: Karoo
(low-Ti)
Rocks vs. chondrite
1000
100
10
1
La Ce Pr Nd Sm Eu Gd Tb Dy Ho Er Yb Lu

Figure 5

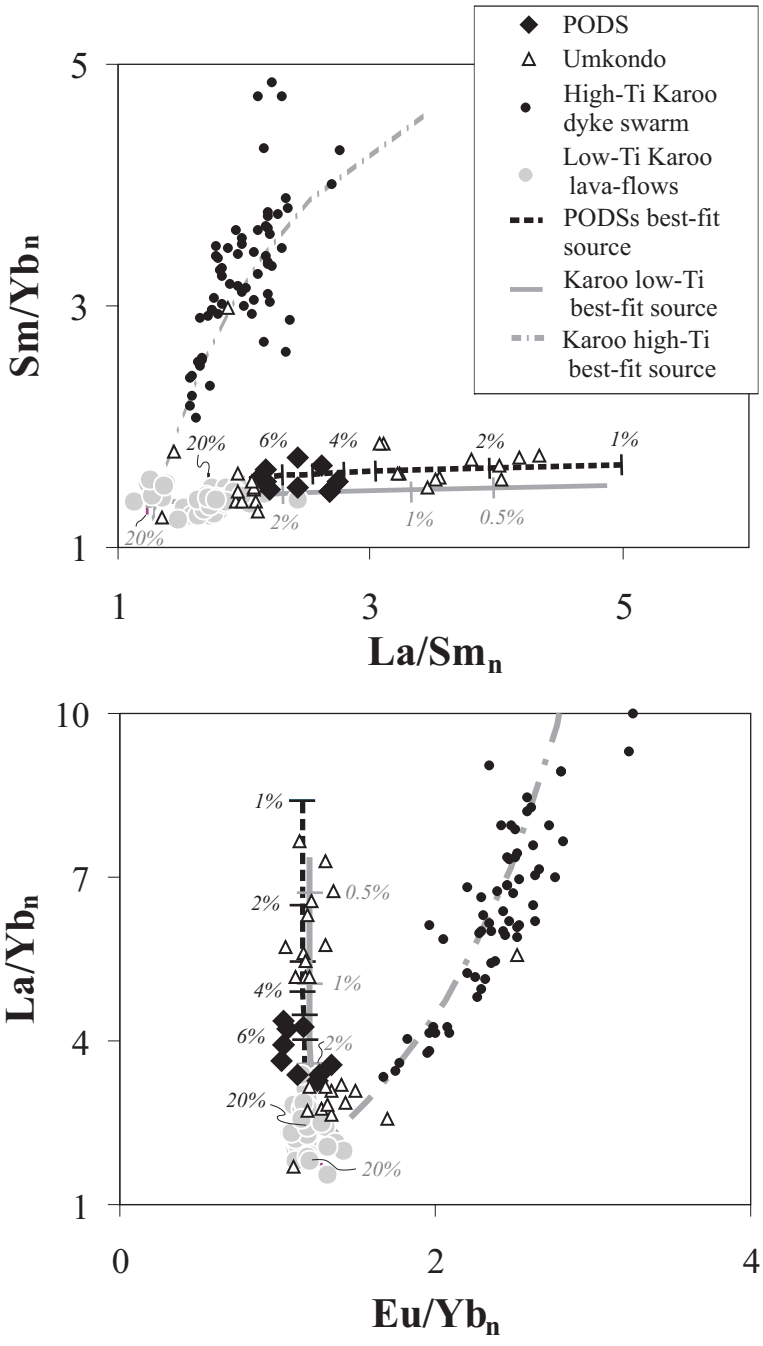
PODS
Umkondo
High-Ti Karoo dyke swarm
Low-Ti Karoo lava-flows
PODSs best-fit source
Karoo low-Ti best-fit source
Karoo high-Ti best-fit source
Sm/Yb$_n$
La/Sm$_n$
La/Yb$_n$
Eu/Yb$_n$
20%
6%
4%
2%
1%
0.5%

Figure 6

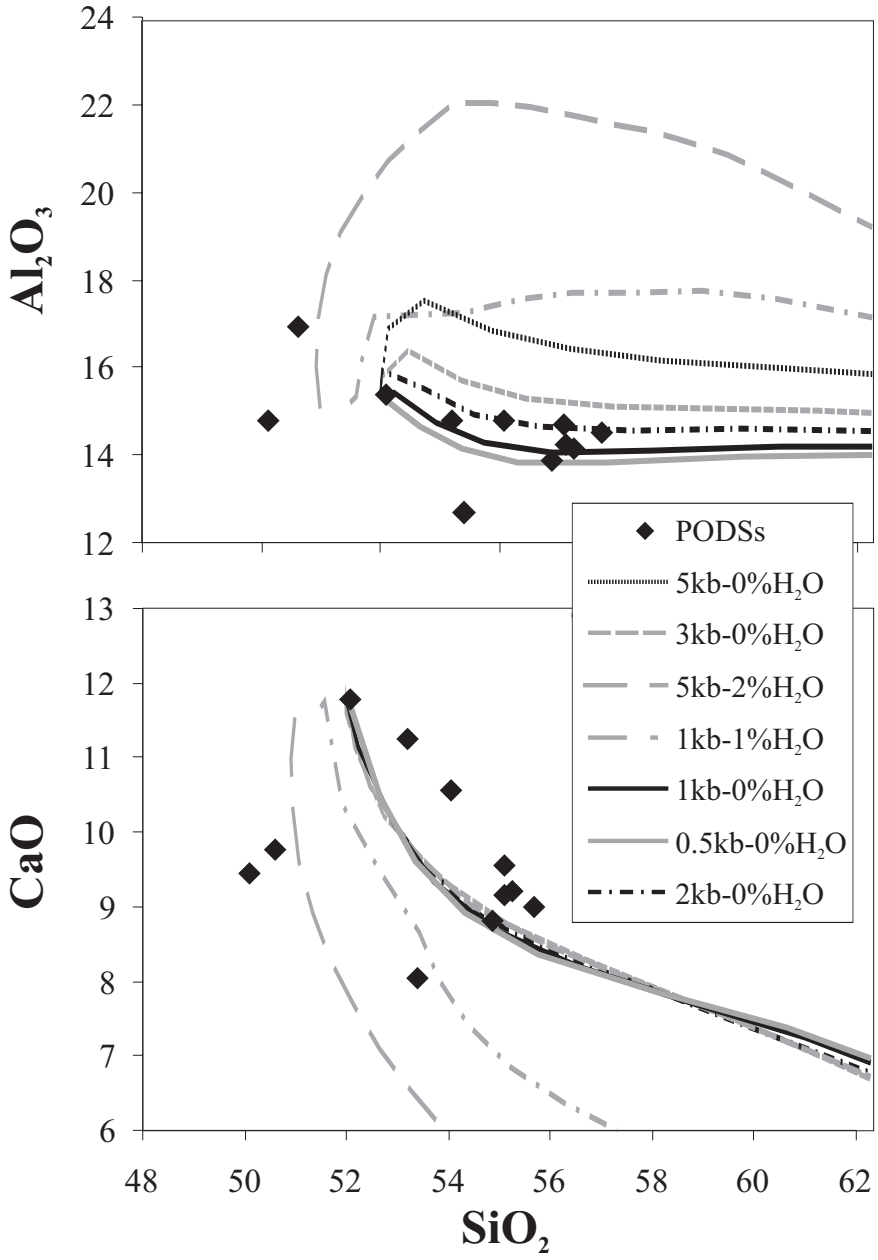

Figure 7: Jourdan et al.

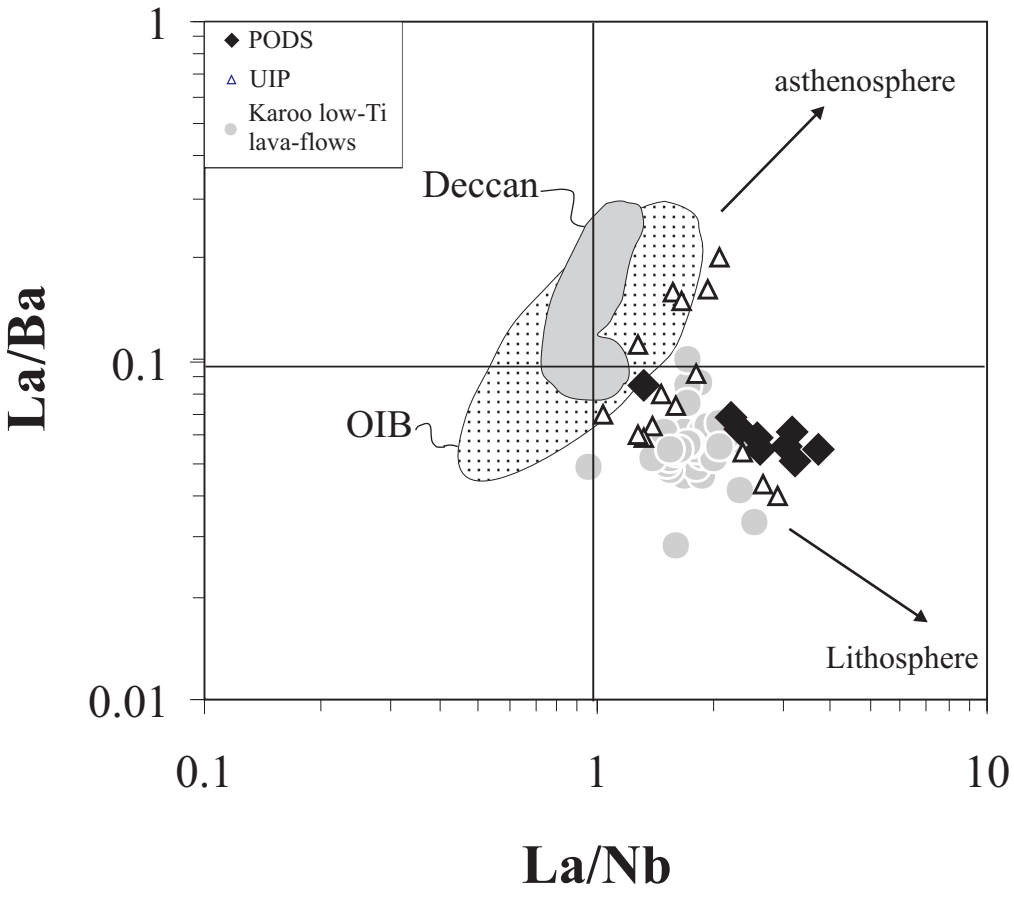
PODS
UIP
Karoo low-Ti lava-flows
Deccan
OIB
asthenosphere
Lithosphere
1
0.1
0.01
0.1
1
10
La/Ba
La/Nb

Figure 8

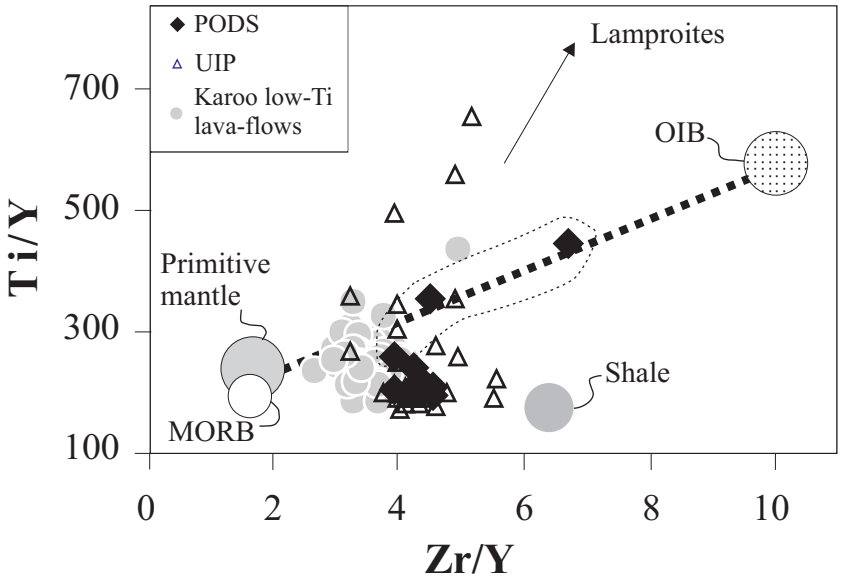
PODS
UIP
Karoo low-Ti lava-flows
Lamproites
OIB
Primitive mantle
MORB
Shale
700
500
300
100
0
2
4
6
8
10
Ti/Y
Zr/Y

Figure 9

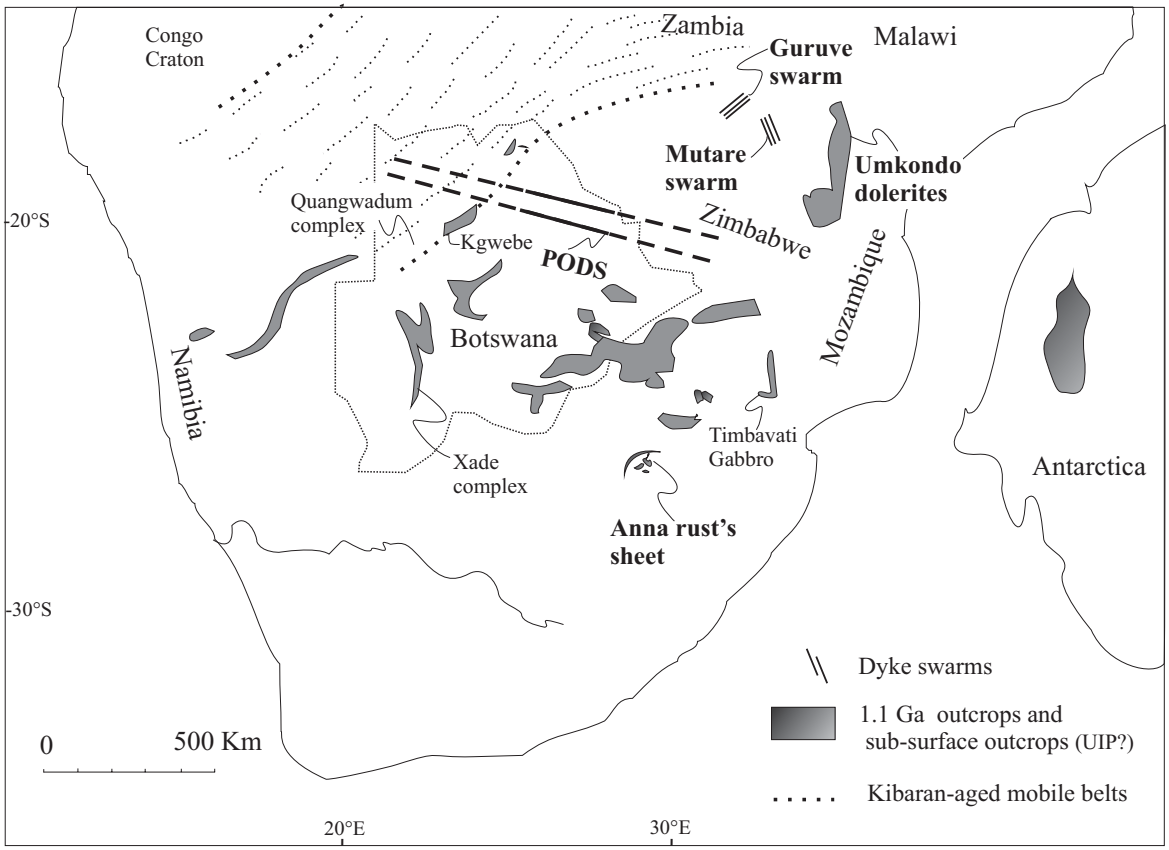
Congo
Craton
Zambia
Malawi
Guruve
swarm
Mutare
swarm
Umkondo
dolerites
Quangwadum
complex
Kgwebe
PODS
Zimbabwe
Mozambique
20°S
Botswana
Namibia
Timbavati
Gabbro
Xade
complex
Anna rust's
sheet
Antarctica
30°S
0
500 Km
20°E
30°E
Dyke swarms
1.1 Ga outcrops and
sub-surface outcrops (UIP?)
Kibaran-aged mobile belts

Figure 10

Type	Sill	Sill	Dyke	Dyke	Dyke	Dyke	Dyke	Dyke	Dyke	Dyke	Sill
Sample	Bot01	Bot11	Bot15A	Bot17	Bot0083	Bot0084	Bot0085	Bot0093	Bot0094	Bot0095	Bot0003
Major elements (wt%)											
SiO_2	52.06	49.49	48.93	52.39	53.31	54.32	53.95	53.42	53.70	53.65	51.09
Al_2O_3	12.36	16.56	14.43	14.54	14.59	14.13	14.37	13.49	13.75	13.85	15.08
Fe_2O_3	16.36	12.89	15.09	9.95	11.11	11.76	11.54	11.43	12.19	11.96	9.92
MgO	3.91	4.49	5.74	8.20	6.32	4.75	5.20	6.19	4.94	5.15	8.20
CaO	7.84	9.54	9.23	11.09	10.42	8.78	9.36	8.58	8.95	8.92	11.57
Na_2O	2.67	3.13	2.62	1.98	1.86	2.06	2.06	2.29	2.15	2.10	1.68
K_2O	1.39	0.92	0.87	0.63	1.04	1.65	1.39	1.87	1.48	1.69	0.58
TiO2	2.09	1.70	1.85	0.50	0.82	0.97	0.94	0.94	0.96	0.93	0.73
P_2O_5	0.23	0.17	0.20	0.06	0.09	0.12	0.11	0.09	0.11	0.11	0.08
MnO	0.21	0.18	0.21	0.16	0.17	0.17	0.17	0.18	0.19	0.18	0.17
LOI	0.51	0.89	0.62	0.93	0.51	1.14	1.17	0.88	1.35	1.42	0.83
H2O-	0.18	-	0.18	-	0.13	0.17	0.09	0.90	0.18	0.21	-
TOTAL	99.81	99.96	99.97	100.43	100.37	100.02	100.35	100.26	99.95	100.17	99.93
Mg#	35.77	44.81	46.99	65.76	57.00	48.49	51.22	55.79	48.57	50.09	65.83
Trace elements (ppm)											
Rb	54	27	29	36	*47*	77	64	*99*	67	87	21
Ba	351	261	215	163	*219*	351	320	*473*	309	343	152
Th	6.48	3.50	3.67	3.06	-	6.38	5.62	-	6.19	5.91	2.72
Nb	10.24	8.12	8.61	2.92	*3.40*	6.10	5.33	*4.30*	5.65	5.42	3.20
Sr	142	188	161	129	*118*	131	132	*197*	135	134	132
Hf	5.27	3.76	4.05	1.72	-	3.61	3.19	-	3.33	3.30	2.26
Zr	182	139	147	68	*95*	122	113	*99*	114	122	91
Y	47.2	32.1	35.7	15.2	*24.2*	30.1	26.8	*20.9*	28.2	27.5	17.2
Pb	10.59	6.79	7.04	9.59	-	7.36	9.37	-	10.12	79.46	7.23
Ta	0.79	0.59	0.61	<0.5	-	<0.5	<0.5	-	<0.5	<0.5	<0.5
U	1.30	0.71	0.64	0.77	-	1.24	1.08	-	1.09	1.09	0.56
Sc	*33*	*33*	*31*	*31*	*32*	*36*	*31*	*26*	*34*	*33*	*30*
V	*406*	*336*	*328*	*208*	*239*	*247*	*249*	*227*	*255*	*252*	*206*
Cr	*7*	*87*	*100*	*222*	*109*	*50*	*69*	*185*	*32*	*28*	*216*
Co	*49*	*37*	*38*	*47*	*50*	*45*	*45*	*47*	*47*	*47*	*44*
Ni	*52*	*48*	*55*	*128*	*97*	*76*	*83*	*69*	*70*	*78*	*104*
La	24.11	16.32	15.09	17.78	10.09	-	19.51	17.34	17.22	17.33	9.19
Ce	52.50	33.61	32.45	37.22	21.06	-	42.92	36.83	39.20	38.88	19.59
Pr	7.14	4.70	4.48	5.10	2.69	-	5.16	4.60	4.66	4.60	2.63
Nd	28.16	18.69	18.02	20.21	9.98	-	19.77	17.03	18.11	18.03	10.03
Sm	7.10	4.71	4.51	5.23	2.31	-	4.68	4.07	4.36	4.05	2.65
Eu	1.85	1.48	1.36	1.57	0.59	-	1.11	1.09	1.08	1.08	0.77
Gd	7.46	5.27	5.00	5.82	2.44	-	4.88	4.35	4.65	4.51	2.90
Tb	1.18	0.85	0.80	0.89	0.40	-	0.77	0.68	0.73	0.69	0.47
Dy	7.59	5.14	4.81	5.59	2.36	-	4.57	4.21	4.40	4.33	2.85
Ho	1.69	1.22	1.13	1.28	0.54	-	1.03	0.98	1.03	1.03	0.63
Er	4.80	3.28	3.19	3.53	1.59	-	2.94	2.80	2.77	2.78	1.73
Yb	4.85	3.35	3.16	3.58	1.64	-	3.04	2.97	2.72	3.01	1.70
Lu	0.73	0.50	0.47	0.53	0.25	-	0.47	0.42	0.45	0.44	0.27

Table 1: Jourdan et al.